Comparison of Centered Discrete Fractional Fourier Transforms for Chirp Parameter Estimation

D. Jackson Peacock and Balu Santhanam
Department of Electrical and Computer Engineering
University of New Mexico, Albuquerque, NM USA, 87131
Email: jpeacock,bsanthan@unm.edu

***Abstract*—The Discrete Fractional Fourier Transform (DFRFT) is a promising tool for multicomponent chirp parameter estimation. Computation of this transform and its chirp concentration properties are dependent on the basis of DFT eigenvectors used in the computation. Several DFT-eigenvector basis have been proposed for the transform and there is no common framework for comparing them. Furthermore, the analysis done in all prior work completely ignore the presence of noise. In this paper, we compare different versions of the transform using statistical consistency of the chirp parameter estimators as the criteria. Their impact on estimation errors, is evaluated by comparing them to the Cramer-Rao lower bound, with both conventional and recent super-resolution subspace extensions of the technique.**

Keywords: Discrete Fractional Fourier Transform, chirp parameter estimation, peak to parameter mapping, consistency criteria, subspace techniques.

I. Introduction

The Fractional Fourier Transform (FrFT) is a rotational generalization of the traditional Fourier Transform [1]. The eigenfunctions of the continuous FrFT are the Gauss-Hermite (G-H) functions, which result in a kernel composed of chirps. Consequently the application of the FrFT to a chirp results in an impulse at a specific angle and location corresponding to its chirp rate and center frequency, as given by closed-form equations. This has motivated research into discrete versions of the transform which can be used for chirp parameter estimation.

Discrete versions of the FRFT have been developed by several researchers and can be put into the general form [2]:

$$\mathbf{X}_a = \mathbf{W}^{\frac{2a}{\pi}}\mathbf{x} = \mathbf{V}\mathbf{\Lambda}^{\frac{2a}{\pi}}\mathbf{V}^T\mathbf{x}, \tag{1}$$

where $\mathbf{W}$ is a DFT matrix, $\mathbf{V}$ is a matrix of DFT eigenvectors and $\mathbf{\Lambda}$ is a diagonal matrix of DFT eigenvalues. This requires the furnishing of a full basis of DFT eigenvectors: $\mathbf{V}$. However, there is no unique prescription for this basis, leading to the many proposed forms. The search for DFT eigenvectors has focused on using matrices that commute with the DFT matrix and thus have the same eigenvectors. A matrix found by Dickenson and Steiglitz (D-S) was investigated first [3], followed later by a matrix found by Grünbaum [4]. Recently, another commuting matrix was proposed using techniques developed for quantum mechanics in finite dimensions (QMFD) [5]. Numerous other bases have also been proposed by combining or adapting these. A fast algorithm for computing the DFRFT using any of these approaches has been outlined in [6]. The DFRFT is a promising tool for chirp parameter estimation and vibration detection and estimation in SAR applications [7].

This work was supported by the US Department of Energy (award no. DE-FG52-08NA28782) and by the National Science Foundation (award no. IIS-0813747).

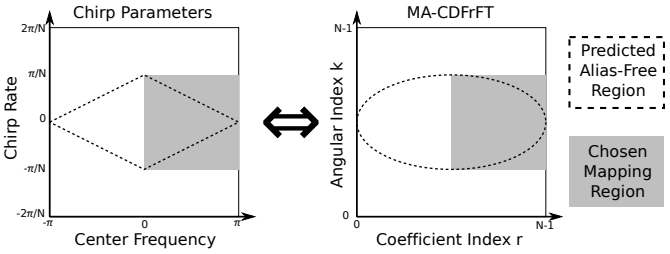

Fig. 1. Expected Valid Mapping Region: Outside of the dashed region, the instantaneous frequency of chirps spills out of $\omega \in [-\pi, \pi]$, so the Nyquist sampling theorem is not satisfied. Mappings are generated for the region shown in grey.

All the proposed sets of eigenvectors for the DFrFT are approximations of the G-H functions, and thus the application of the DFrFT to a sampled chirp results in a strong peak in the 2D plane. However, unlike the continuous version, there are no known closed-from solutions for the mapping between the transform peak location and chirp parameters. Prior work has assumed this mapping is a sampled version of the mapping for the continuous FrFT, but this is only accurate for very narrowband chirps, and not suitable for wideband signals. Furthermore, performance analysis for existing DFRFT approaches has been done in the absence of noise.

In this paper, we compute the peak to parameter mappings [8] associated with the three DFrFT bases, and in the process, show that these mappings are considerably different from each other. Furthermore, using statistical consistency related criteria, we show that they are not invertible over the full range of the transform. This leads to inconsistent estimates for chirp parameters outside the invertible regions, where the estimation error increases significantly. Finally, we evaluate the impact of these criteria on the efficiency of chirp parameter estimates of the different basis, by comparing the MSE of the approaches to the Cramer-Rao lower bound.

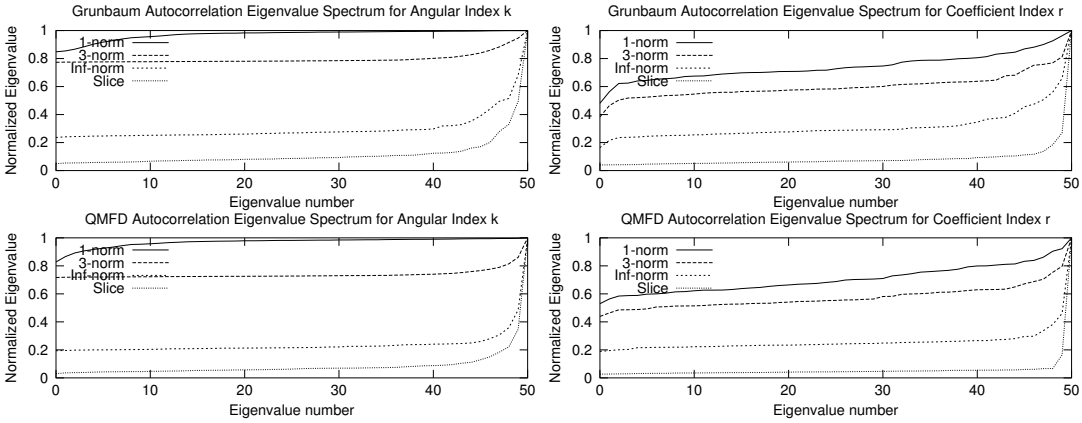

Fig. 2. Autocorrelation matrix eigenvalues: The eigenvalues of the autocorrelation matrix of projections of the MA-CDFrFT of a complex-valued single-component noise-free chirp signals of length $N = 256$ for both the Grunbaum and QMFD basis. The autocorrelation matrix is estimated using the pre-windowed padding option. The cross-hair subspace technique in conjunction with the QMFD approach produces the largest separation between the signal and noise subspaces.

II. Peak to Parameter Mapping

The chirp model used in this paper is formulated as:

$$s[n] = \exp(j(\alpha(n-(N-1)/2)^2 + \omega n)) + w[n], \quad (2)$$

where α is the chirp rate, ω is the center frequency, $0 \leq n \leq N-1$ and $w[n]$ is additive Gaussian white noise.

To calculate the peak-to-parameter mappings, we generated $4N \times 4N$ sample chirp functions evenly spaced in the range $\alpha \in (0, \pi)$ and $\omega \in (-\pi/N, \pi/N)$, as shown in Fig. 3(a). The peaks in the DFrFT for these chirps occur roughly between k = N/4 to 3N/4 and r = N/2 to N, thus on average 64 chirps mapped to each peak location in the transform.

Application of the DFrFT to chirp parameter estimation is not meaningful if a complete analysis of the invertibility of this mapping is ignored. Figure 3 (b,c,d) illustrates a contour plot of the peak-to-parameter mapping for the different transforms resulting from using the different eigenvector basis. In the Grünbaum mapping the contour lines become diffuse when the IF of the chirp exceeds the limits specified by the sampling theorem, indicating that the mapping is not monotonic in that region. The two ovoid shapes in the high frequency end of the D-S plot are caused by the side-lobes of the peak obtaining greater magnitude than the "peak" itself. These regions were masked out during further analysis to avoid spilling over into other regions. The QMFD mapping is closest to the continuous mapping, in fact for $\omega < \pi/3$ a sampled version of the closed-form continuous mapping is just as accurate as the mapping we computed:

$$\alpha = -\frac{\pi}{N}\cot\left(\frac{k\pi}{N}\right), \omega = \frac{2\pi}{N}\left(r - \frac{N-1}{2}\right)\csc\left(\frac{k\pi}{N}\right).$$

The mappings were inverted by calculating the centroid of all chirp parameters that map to the same peak location. This inversion is not meaningful, however, if the mapping is not monotonic. To be a monotonic mapping in two dimensions [8]: (a) the set of all chirp parameters that map to a single location in the chirp-rate vs center-frequency plane must form a connected set, and (b) locations which are adjacent in the transform space must map to adjacent regions in the chirp parameter space. Prior work with the DFrFT and its application to chirp parameter estimation has mainly focussed on just a specific chirp parameter set.

Figure 4 depicts the regions in the α–ω plane where the mappings satisfied the connectivity and adjacency conditions. The invertible mapping regions for the D-S basis shows several regions where the connectivity criteria are not met. The mapping for the Grunbaum basis depicts a significantly smaller invertible region in comparison to the diamond shaped region, where aliasing does not occur. This is attributable to the adjacency criteria being violated. The QMFD basis satisfies these two consistency conditions over a much larger region, exerting fewer constraints on the range of chirps with which it can be used.

III. Performance Evaluation

Figure 5 shows the chirp parameter estimation errors using simple 2D peak detection in MA-CDFrFT transform plane. When the SNR is very low, the performance of all methods is similar. When the SNR is high, the average error is roughly the same as the resolution of the transform. However, the D-S basis results in significantly more error. This is because the peak to parameter mapping depicts multiple disconnected regions of chirp parameters mapping to the same peak location. Consequently the variance of the estimators for those locations is much higher than in the other mappings where only a tightly clustered connected region of chirp parameters maps to each peak location.

The structure of the mapping can have even more of a significant effect on super-resolution estimations. To quantify this we use a cross-hairs subspace decomposition technique investigated in [8] to refine the estimate. In this method, existing subspace decomposition techniques are applied to the row and column of the transform containing the peak providing super-resolution peak locations. The computed mapping is then

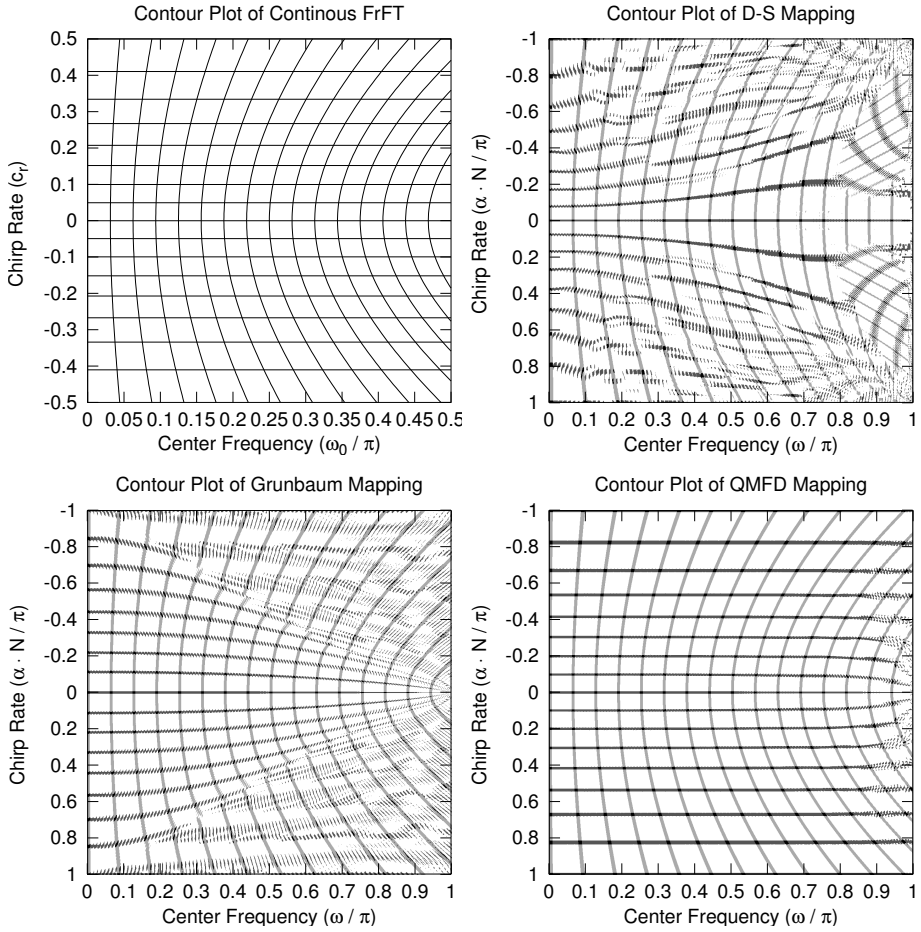

Fig. 3. Contour Plots of Computed Mappings: (a) continuous FRFT mapping where each contour line shows the locus of chirp parameters mapping to a single angle or location in the continuous FrFT space. Contours are drawn for angles $\alpha \in [\frac{\pi}{4}, \frac{3\pi}{4}]$ in $\frac{\pi}{32}$ increments, at center-frequency locations in $[0, \frac{\pi}{2}]$ in $\frac{\pi}{32}$ increments. This corresponds to the grey region in Fig. 1, (b,c,d) contour plots of the mapping for the different basis, where each contour "line" shows the locus of chirp parameters that map to a single row or column of an $N = 256$ size transform. Contours are drawn for every 8th row and column, with contours for $64 \leq k \leq 192$ and $128 \leq r \leq 248$ visible. The area shown corresponds to the grey region shown in Fig. 1(a)

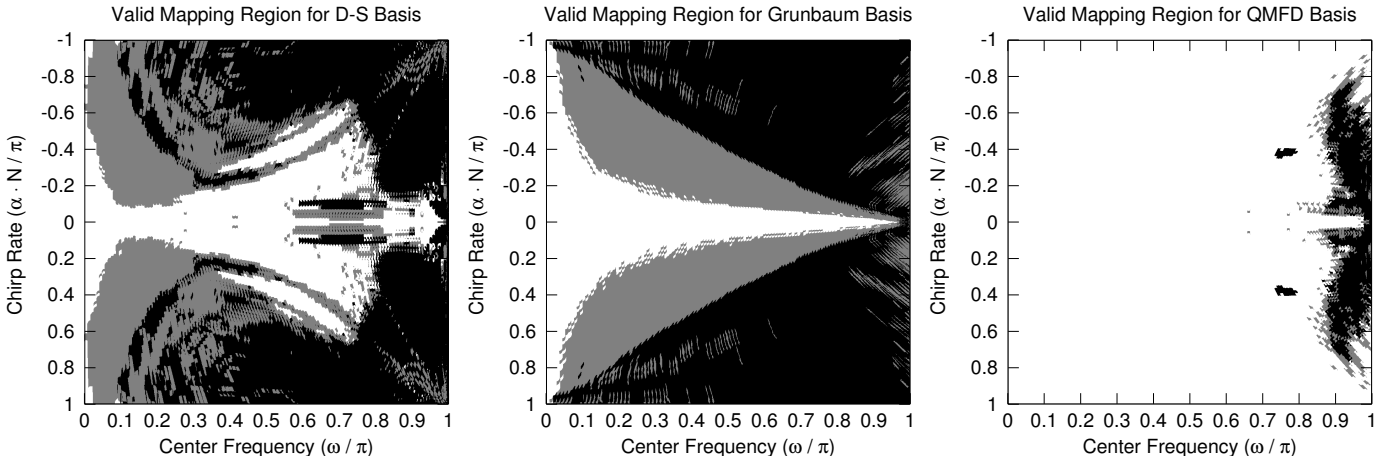

Fig. 4. Actual Valid Mapping Regions: Black regions depict where the connectivity criteria is not satisfied. Grey regions depict where the adjacency criteria is not satisfied. White regions indicate that both criteria are satisfied. The mappings are for chirps of length $N = 256$, with a transform size of $N \times N$, measured using $4N \times 4N$ chirps with center frequencies and chirp rates evenly spaced over the shown area.

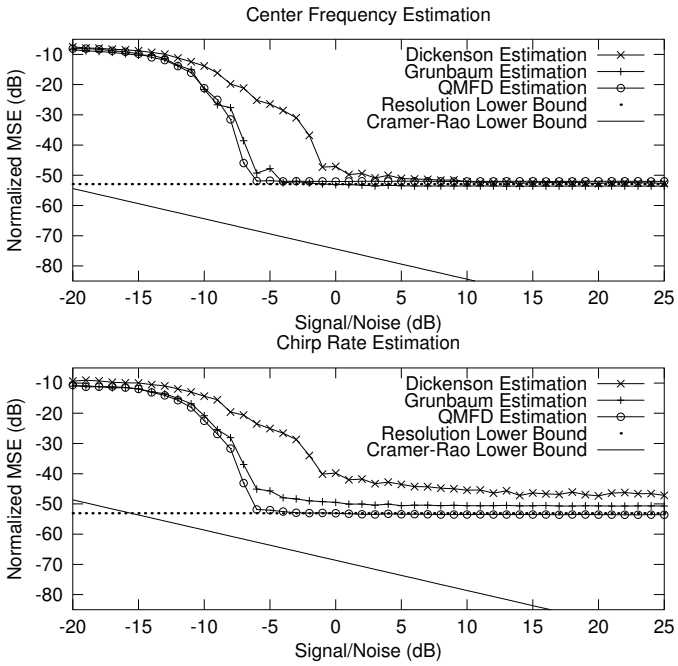

Fig. 5. 2D Peak Detection Estimation Error: The MSE was calculated at each SNR using 1000 chirps of length $N = 256$, in the "safe" range of $|\alpha|(N-1) + |\omega| = \text{IF} < 0.85\pi$. A transform of size $N \times N$ was used.

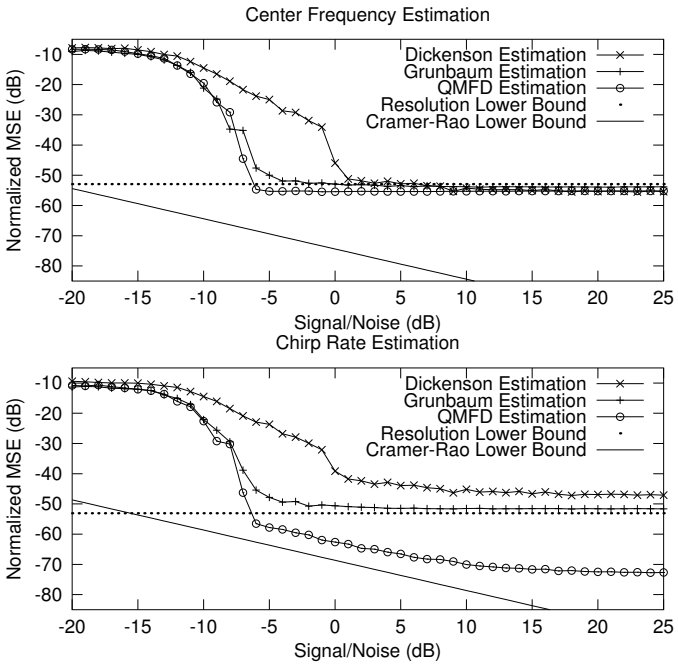

Fig. 6. Cross-Hairs Estimation Error: The MSE was calculated at each SNR using 1000 chirps of length $N = 256$, in the "safe" range of $\text{IF} < 0.85\pi$. A transform of size $N \times N$ was used, refined using minimum norm subspace decomposition and FFT size $R = 8192$.

linearly interpolated to provide an estimate of the chirp parameters. Fig. (2) depicts the eigenvalues for the autocorrelation matrices associated with the center-frequency and chirp-rate projections indicating that the cross-hairs technique provides significantly better signal and noise subspace separation than in prior work [8].

Figure 5 and Fig. (6) depict the chirp parameter estimation errors using the 2D peak picking and cross-hairs subspace techniques respectively. As is evident, either of these techniques has more success using the QMFD basis. This is attributable to the fact that satisfying the adjacency property implies that interpolating the mapping is a more meaningful operation. The other contributing factor is the fact that the chirp rate estimation problem is separable from the center-frequency estimation problem in this basis, as seen in Fig. 3, where the chirp-rate contour lines are approximately horizontal parallel lines.

IV. Conclusion

In this paper, we have shown that the different bases of DFT eigenvectors proposed for the computation of the Centered Discrete Fractional Fourier Transform are not equally appropriate for application towards the problem of wideband chirp parameter estimation. It was shown using connectivity and adjacency criteria applied to their underlying peak to parameter mappings, that each of these methods have very different validity regions where the resulting chirp parameter estimates are consistent.

Properties leading to inconsistent parameter estimates were shown to have a measurable impact on the estimation error at fixed transform sizes. It was further shown that among the three DFT eigenvector basis studied, the QMFD basis resulted in: (a) the largest set of chirp parameters, where the adjacency and connectivity criteria for the peak to parameter mapping are satisfied, (b) peak to parameter mappings that are the closest to the corresponding continuous FRFT parameter mappings. The smallest chirp parameter estimation errors in turn resulted when the QMFD basis was deployed in conjunction with the subspace cross-hair technique.

References

[1] L. B. Almeida, "An introduction to the angular Fourier transform," in *Proc. of ICASSP*, vol. 3, Apr. 1993, pp. 257 –260.

[2] B. Santhanam and J. H. McClellan, "The discrete rotational Fourier transform," *IEEE Trans. on Sig. Proc.*, vol. 44, no. 4, pp. 994 –998, Apr. 1996.

[3] B. Dickinson and K. Steiglitz, "Eigenvectors and functions of the discrete Fourier transform," in *IEEE Trans on ASSP*, vol. 30, no. 1, Feb. 1982, pp. 25 – 31.

[4] S. Clary and D. H. Mugler, "Shifted Fourier matrices and their tridiagonal commutors," *SIAM J. Matrix Anal. Appl.*, vol. 24, no. 3, pp. 809–821, 2003.

[5] B. Santhanam and T. S. Santhanam, "On discrete Gauss-Hermite functions and eigenvectors of the discrete Fourier transform," *Signal Processing*, vol. 88, no. 11, pp. 2738 – 2746, 2008.

[6] J. G. Vargas-Rubio and B. Santhanam, "On the multiangle centered discrete fractional Fourier transform," *IEEE Sig. Proc. Letters*, vol. 12, no. 4, pp. 273 – 276, Apr. 2005.

[7] Q. Wang, M. Pippen, R. J. Beach, R. Dunkel, B. Santhanam, B. Santhanam, A. Doerry, and M. M. Hayat, "Sar-based vibratiton estimation using the discrete fractional fourier transform," *IEEE Trans. Geo., Sci., Rem., Sens.*, vol. 50, no. 10, pp. 4145–4156, Oct. 2011.

[8] D. J. Peacock and B. Santhanam, "Multicomponent subspace chirp parameter estimation using discrete fractional Fourier analysis," in *Proc. of IASTED SIP*, Dec. 2011, pp. 326–333.